

# Exploring the effects of a double reconstruction on the geometrical parameters of coupled models, using observational data

Freddy Cueva Solano

*Instituto de Física y Matemáticas, Universidad Michoacana de San Nicolás de Hidalgo  
Edificio C-3, Ciudad Universitaria, CP. 58040, Morelia, Michoacán, México.\**

(Dated: May 4, 2018)

In this work we study the effects of the non-gravitational exchange energy ( $Q$ ) between dark matter ( $DM$ ) fluid and dark energy ( $DE$ ) fluid on the background evolution of the cosmological parameters. A varying equation of state (EOS) parameter,  $\omega$ , for  $DE$  is proposed. Considering an universe spatially flat, two distinct coupled models were examined to explore the main cosmological effects generated by the simultaneous reconstruction of  $Q$  and  $\omega$  on the shape of the jerk parameter,  $j$ , through a slight enhancement or suppression of their amplitudes with respect to uncoupled scenarios, during its evolution from the past to the near future. In consequence,  $j$  could be used to distinguish any coupled  $DE$  models. Otherwise, the observational data were used to put stringent constraints on  $Q$  and  $\omega$ , respectively. In such a way, we used our results as evidences to search possible deviations from the standard concordance model ( $\Lambda$ CDM), examining their predictions and improving our knowledge of the cosmic evolution of the universe.

PACS numbers: 98.80.-k, 95.35.+d, 95.36.+x, 98.80.Es

## I. INTRODUCTION

The recent astronomical measurements of type Ia Supernovae Union 2.1 (Union 2.1 SNIa) composed by 580 data [1–4], the Baryon Acoustic Oscillation (BAO) detected in the clustering of the combined 2dF Galaxy Survey (2dFGRS) and the Sloan Digital Sky Survey (SDSS) Data Release 7 (DR 7) main galaxy samples, the 6dF Galaxy Survey (6dFGS) and the WiggleZ Dark Energy Survey (WiggleZ) [5–9], the observations of polarization and anisotropies in the power spectrum of the Cosmic Microwave Background (CMB: distance priors) data from the Wilkinson Microwave Anisotropy Probe 7 year (WMAP 7) [10–13], the observational Hubble (H) data set measured from galaxy surveys [14–18], and other, have confirmed that the present universe is undergoing an accelerated phase of expansion. In the literature, some theoretical approaches were taken into account to explain this phenomenon, we are interested in an universe in where exists an exotic energy component with negative pressure, named  $DE$  [19–22], and which presumably began to dominate the evolution of the universe, only recently. Within this approach, the simplest candidate for  $DE$  is the Cosmological Constant  $\Lambda$ , which has an EOS parameter  $\omega = -1.0$  [23–26]. Also, there exist other alternative models such as phantom model [27], quintom model [28], quintessence model [29], the k-essence model [30], Chaplygins gas model [31], massive scalar field model [32] and other. All these models predict different dynamics of the universe.

On the other hand, the properties of  $DE$  are mainly characterized by  $\omega$ . In such a way, due to our ignorance of its nature, it was parameterize empirically in a model independent way. In this sense, we have followed two ways

to explore its behaviour. The first one was to parameterize  $\omega$  in terms of some free parameters [33–37]. Among all the different parametrizations forms the Chevallier-Polarski-Linder (CPL) parametrization [34] is considered as the most popular ansatz  $\omega = \omega_o + \omega_1[z/(1+z)]$ , where  $z$  is the redshift and  $\omega_o, \omega_1$  are real parameters [34]. This ansatz has a divergence problem, when redshift  $z$  approaches to  $-1$  [38]. In addition, some non-parametric forms were found in [39]. The second one was to choose an appropriated local basis representation for  $\omega$  and after estimate the associated coefficients [40–43]. However, a divergence-free reconstruction for  $\omega$  was proposed here, expanding  $\omega$  in terms of the Chebyshev polynomials  $T_n, n \in N$ . To display how the method runs  $\omega$  was expanded in terms of only the first three Chebyshev polynomials  $T_n, n = 0, 1, 2$ , and therefore, they are considered as a complete orthonormal basis on the finite interval  $[-1, 1]$ , and besides, belong to the Hilbert space  $L^2$  of real values [44]. They were chosen because have the property to be the minimal approximately polynomials [16, 45].

On the other hand, within the universe another dark component has been assumed its existence, so-called  $DM$ , which acts exactly like the ordinary matter (pressureless), but does not interact with  $DE$ , except gravitationally. The nature of these dark components are not still known and the possibility that within the universe exists a non-gravitational coupling in the dark sector could not be precluded, as well as, its possible effect on the dynamics evolution of the cosmological parameters should be considered [46–59]. Some consequences of it were already studied in [60–63], from which the strenght of the coupling should be very small.

A huge amount of coupled  $DE$  models have already been investigated and fitted with cosmological data. Some of them were motivated by mathematical simplicity, for example, models in which  $Q \propto H\rho$ , in where  $H$  and

\* freddy@ifm.umich.mx, freddycuevasolano2009@gmail.com

$\rho$  denote the Hubble parameter and the energy density of dark sectors, respectively. It has three possibilities, namely,  $\rho = \rho_{DM}$  ( $DM$  energy density),  $\rho = \rho_{DE}$  ( $DE$  energy density) and  $\rho = \rho_{DM} + \rho_{DE}$  [59]. On the contrary, the models with  $Q \propto \rho$  have been used in reheating [46], curvaton decay [47] and decay of  $DM$  into radiation [48]. All these models strongly depend on the choice made for the  $Q$  form. So far, the coupled  $DE$  models have not been investigated, in a general form before. In effect, some attempt to reconstruct  $Q$  from a general parametrization has been done by us in [64]. In this paper we have considered different theoretical scenarios, in where  $\omega$  was always taken as constant. Here, we fixed  $Q \propto HI_Q(1+z)^3$ , where the function  $I_Q$  was reconstructed in terms of the first six Chebyshev polynomials. The analysis was done using a sample of SNIa Union 2 data. Our main results showed that the best fitted on  $I_Q$  have preferred to cross the noncoupling line  $I_Q = 0$  during its evolution.

The motivation of this article has been to go from theory to observations, following the prescription outlines by Cueva-Nucamendi [64]. Then, to follow this thread, a coupled model with two reconstructions describing to  $Q$  and  $\omega$  simultaneously has been proposed here. Therefore, we have postulated the existence of a general non-gravitational coupling between  $DE$  and  $DM$  [64], introducing a general phenomenological parametrization for  $Q$  into the equations of motion of these dark components. Here,  $Q$  was reconstructed expanding it in terms of the first three Chebyshev polynomials  $T_n$ ,  $n = 0, 1, 2$ . This has been the first attempt at reconstructing simultaneously  $Q$  and  $\omega$  from real data.

Two distinct coupled  $DE$  models such as XCPL and DR were analysed here. Within these scenarios, the aim of our paper has been to study the effects that result from the reconstructions of  $Q$  and  $\omega$  on the cosmological background evolution, of some parameters such as (defined below)  $DM$  energy density parameter ( $\Omega_{DM}$ ), deceleration parameter ( $q$ ) and jerk parameter ( $j$ ) [65–70], whose amplitudes are modified with respect to those of uncoupled models. Here, our models were constrained using an analysis combined of Union 2.1 SNIa [1–4], BAO [5–9], CMB [10–13], and H data sets [14–18].

Finally, we organize this paper as follows: The background equation of motions for the energy densities, the definition of the geometrical parameters, and the reconstruction schemes for  $Q$  and  $\omega$  are derived in section II. In section III we describe the coupled  $DE$  models worked. The priors considered and the observational constraints on the parameters space are discussed in section IV. We discuss our results in section V. In section VI we conclude our main results.

## II. BACKGROUND EQUATIONS OF MOTION

In a flat Friedmann-Robertson-Walker (FRW) universe its background dynamics is described by the following set

of equations for their energy densities (detailed calculations are found in [64], so we do not discuss them here.)

$$\dot{\rho}_b + 3H \rho_b = 0, \quad (1)$$

$$\dot{\rho}_r + 4H \rho_r = 0, \quad (2)$$

$$\dot{\rho}_{DM} + 3H \rho_{DM} = +Q, \quad (3)$$

$$\dot{\rho}_{DE} + 3(1+\omega) H \rho_{DE} = -Q, \quad (4)$$

where  $\rho_b$ ,  $\rho_r$ ,  $\rho_{DM}$  and  $\rho_{DE}$  are the energy densities of the baryon, radiation,  $DM$  and  $DE$ , respectively. Now defined the Hubble expansion rate as  $H \equiv \dot{a}/a$ , and also, “.” indicates differentiation with respect to the time  $t$ .

In what follows we shall assume that there is not energy transfer from  $DE$  ( $DM$ ) to baryon or radiation, and among them only exist a gravitational coupling [71]. The critical densities  $\rho_c \equiv 3H^2/8\pi G$ , and the critical density today  $\rho_{c,0} \equiv 3H_0^2/8\pi G$ , in where  $H_0$  is the current value of the Hubble parameter, were conveniently defined. Considering that  $A = b, r, DM, DE$ , then the normalized densities are

$$\Omega_A \equiv \frac{\rho_A}{\rho_c} = \frac{\rho_A/\rho_{c,0}}{\rho_c/\rho_{c,0}} = \frac{\Omega_A^*}{E^2}, \quad \Omega_{A,0} \equiv \frac{\rho_{A,0}}{\rho_{c,0}}. \quad (5)$$

The first Friedmann equation is then given by

$$E^2 \equiv \frac{H^2}{H_0^2} = \frac{8\pi G}{3H_0^2} (\rho_b + \rho_r + \rho_{DM} + \rho_{DE}), \\ = [\Omega_b^* + \Omega_r^* + \Omega_{DM}^* + \Omega_{DE}^*], \quad (6)$$

and with the following relation for all time

$$\Omega_b + \Omega_r + \Omega_{DM} + \Omega_{DE} = 1. \quad (7)$$

The scale factor  $a$  is related with the redshift through  $a = 1/(1+z)$ , from which find  $dt/dz = -1/(1+z)H(z)$ . By substituting this last relation into Eqs. (1)-(4), and solving Eqs. (1)-(2), find the redshift evolution of  $\Omega_A^*$

$$\Omega_b^*(z) = \Omega_{b,0}(1+z)^3, \quad (8)$$

$$\Omega_r^*(z) = \Omega_{r,0}(1+z)^4, \quad (9)$$

$$\frac{d\Omega_{DM}^*}{dz} - \frac{3\Omega_{DM}^*}{1+z} = \frac{-\Omega_{DM}^* I_Q(z)}{1+z}, \quad (10)$$

$$\frac{d\Omega_{DE}^*}{dz} - \frac{3(1+\omega)\Omega_{DE}^*}{1+z} = \frac{+\Omega_{DM}^* I_Q(z)}{1+z}. \quad (11)$$

Then, these equations have been fundamental to determine the results within our models.

### A. Evolution of geometrical parameters

The geometrical parameters of the universe are obtained by performing a Taylor series expansion of the scale factor  $a(t)$  around the current epoch,  $t_0$ . Conventionally, this series is truncated at a determined order [65]. Then, in this work we have been truncated such series at third order to study its behaviour, in where the

dimensionless coefficients such as deceleration parameter,  $q$ , and jerk parameter,  $j$ , are defined as [65]:

$$q(z) \equiv -\frac{1}{H^2} \frac{\ddot{a}}{a} = -1 + \frac{(1+z)}{H(z)} H'(z), \quad (12)$$

$$j(z) \equiv +\frac{1}{H^3} \frac{\dddot{a}}{a} = q(z) + 2q^2(z) + (1+z)q'(z), \quad (13)$$

where  $\ddot{a}$  and  $\dddot{a}$  are the second and third derivatives of  $a$  with respect to time, respectively, and also, “ $'$ ” indicates differentiation with respect to  $z$ . Besides, some authors define the jerk parameter,  $j$ , with opposite sign [65, 67, 70]. Let us substitute Eqs. (5)-(7) into Eq. (12),

$$q(z) = +\frac{3}{2}\omega(z)\Omega_{DE}(z) + \frac{1}{2} + \frac{\Omega_r(z)}{2}, \quad (14)$$

and its derivative is

$$q'(z) = +\frac{3}{2}\omega'(z)\Omega_{DE}(z) + \frac{3}{2}\omega(z)\Omega'_{DE}(z) + \frac{\Omega'_r(z)}{2}. \quad (15)$$

These equations are frequently used in this work.

### B. Parametrizations of $Q$ and $w$

The Chebyshev polynomials form a complete set of orthonormal functions on the interval  $[-1, 1]$  and have the property to be the minimal approximating polynomials, which means that have the smallest maximum deviation from the true function at any given order [16, 64].

In general, an energy exchange is described as the coupling between both dark fluids and phenomenologically it is chosen as a rate proportional to  $H$

$$Q \equiv H\rho_{DM}I_Q. \quad (16)$$

Here, the strength of the coupling is characterized by  $I_Q$ ,

$$I_Q \equiv \sum_{n=0}^2 \lambda_n T_n, \quad (17)$$

in where the coefficients of the polynomial expansion  $\lambda_n$  are free dimensionless parameters [64] and

$$T_0(z) = 1, \quad T_1(z) = z, \quad T_2(z) = (2z^2 - 1), \quad (18)$$

represent the first three Chebyshev polynomials.

Within the CPL model, the past evolution history may be successfully described by its EOS parameter,  $\omega$ , but the future evolution may not be explained, because  $\omega$  grows increasingly, and then, encounters a divergence when  $z \rightarrow -1$ . This is not a physical feature. Therefore, a novel reconstruction form for  $\omega$  has been proposed here to avoid such divergence problem. Hence,  $\omega$  is defined as

$$\omega \equiv \sum_{m=0}^2 \omega_m T_m, \quad (19)$$

where  $\omega_0, \omega_1$  and  $\omega_2$  are free dimensionless parameters. The Chebyshev polynomials of order  $m = 2$  were defined by Eq. (18). Using numerical simulations we will compute the best fitted values for  $\lambda_0, \lambda_1, \lambda_2, \omega_0, \omega_1$  and  $\omega_2$ , respectively.

## III. DARK ENERGY MODELS

### A. $\Lambda$ CDM model

In this scenario, the function  $E^2$  was found fixing both  $\omega(z) = -1$  and  $Q(z) = 0$  into Eqs. (8)-(11)

$$E^2 = \left[ \Omega_b^*(z) + \Omega_r^*(z) + \Omega_{DM,0}(1+z)^3 + \Omega_{DE,0} \right], \quad (20)$$

moreover,  $q$  and  $q'$  are given by the Eqs. (14)-(15), then

$$q(z) = +\frac{3}{2} \left[ \Omega_b(z) + \Omega_{DM}(z) \right] + 2\Omega_r(z) - 1, \\ q'(z) = +\frac{3}{2} \left[ \Omega'_b(z) + \Omega'_{DM}(z) \right] + 2\Omega'_r(z), \quad (21)$$

from these equations, reconstructed the parameter  $j(z)$ .

### B. CPL model

Within this model,  $E^2$  was determined replacing both  $\omega(z) = w_o + w_1[z/(1+z)]$ , where  $w_o, w_1$  are real parameters and  $Q(z) = 0$  into Eqs. (8)-(11)

$$E^2 = \left[ \Omega_{b,0}(1+z)^3 + \Omega_{r,0}(1+z)^4 + \Omega_{DM,0}(1+z)^3 \right. \\ \left. + \Omega_{DE,0}(1+z)^{3(1+w_o+w_1)} \exp\left(\frac{-3w_1z}{1+z}\right) \right]. \quad (22)$$

Then, the following relation

$$\omega'(z) = \frac{\omega_1}{(1+z)^2}, \quad (23)$$

is substituted into Eqs. (14)-(15) and (13), from which reconstructed  $q(z)$  and  $j(z)$ , respectively.

### C. XCPL model

Here, firstly a coupled model was defined putting both  $\omega = \omega_o + \omega_1(z/1+z)$ , where  $\omega_o, \omega_1$  are real free parameters and  $Q(z)$  given by Eqs. (16)-(17), into Eqs. (8)-(11). The explicit form for  $\Omega_{DM}^*$  and  $\Omega_{DE}^*$  are reached, solving Eqs. (10)-(11), respectively,

$$\Omega_{DM}^*(z) = (1+z)^3 \Omega_{DM,0} \exp\left[\frac{-z_{max}}{2} \sum_{n=0}^2 \lambda_n I_n(z)\right], \quad (24)$$

$$\Omega_{DE}^*(z) = (1+z)^{3(1+\bar{w})} \left[ \Omega_{DE,0} \exp\left(\frac{-3w_1z}{1+z}\right) + \frac{z_{max}}{2} \Omega_{DM,0} \exp\left(\frac{3w_1}{1+z}\right) \sum_{n=0}^2 \lambda_n S_n(z, \bar{w}) \right]. \quad (25)$$

The following average integrals have been defined

$$\int_0^z \frac{T_n(\tilde{x})}{(1+\tilde{x})} d\tilde{x} \approx \frac{z_{max}}{2} I_n(z), \quad (26)$$

$$\int_0^z \frac{T_n(\tilde{x})A(\tilde{x})B(\tilde{x})}{(1+\tilde{x})^{(1+3\bar{\omega})}} d\tilde{x} \approx \frac{z_{max}}{2} S_n(z, \bar{\omega}), \quad (27)$$

in where we have also defined the following expressions for all  $n \in [0, 2]$  (see Appendix and [64])

$$\begin{aligned} A(\tilde{x}) &= \exp\left(\frac{-z_{max}}{2} \sum_{n=0}^2 \lambda_n I_n(\tilde{x})\right), \\ \tilde{A}(\tilde{x}) &= \exp\left(\frac{-z_{max}}{2} \sum_{n=0}^2 \lambda_n \tilde{I}_n(\tilde{x})\right), \end{aligned} \quad (28)$$

$$B(\tilde{x}) = \exp\left(\frac{-3\omega_1}{1+\tilde{x}}\right), \quad \tilde{B}(\tilde{x}) = \exp\left(\frac{-3\omega_1}{a+b\tilde{x}}\right),$$

$$I_n(z) \equiv \int_{-1}^x \frac{T_n(\tilde{x})}{(a+b\tilde{x})} d\tilde{x},$$

$$S_n(z, \bar{\omega}) \equiv \int_{-1}^x \frac{T_n(\tilde{x})\tilde{A}(\tilde{x})\tilde{B}(\tilde{x})}{(a+b\tilde{x})^{(1+3\bar{\omega})}} d\tilde{x},$$

and the quantities,

$$\begin{aligned} x &\equiv 2(z/z_{max}) - 1, & \bar{\omega} &\equiv \omega_o + \omega_1, \\ a &\equiv 1 + \frac{z_{max}}{2}, & b &\equiv \frac{z_{max}}{2}. \end{aligned}$$

where  $z_{max}$  is the maximum value of  $z$  in which the observations are possible so that  $\tilde{x} \in [-1, 1]$  and  $|T_n(\tilde{x})| \leq 1$ . Therefore, the function  $E^2$  was constructed from Eqs. (8)-(9), (24)-(25) and (6). Similarly, Eq. (23) is then substituted into Eqs. (14)-(15) and (13) to reconstruct  $q(z)$  and  $j(z)$ , respectively.

#### D. DR model

Secondly a coupled model was modeled setting both  $\omega(z) \equiv \omega_o + \omega_1 z + \omega_2(2z^2 - 1)$ , where  $\omega_o, \omega_1, \omega_2$  are real parameters and  $Q(z)$  given by Eqs. (16)-(17), into Eqs. (10)-(11). The explicit form for  $\Omega_{DM}^*$  and  $\Omega_{DE}^*$  are reached, solving Eqs. (10)-(11), respectively. In this way,  $Q$  and  $\omega$  were simultaneously reconstructed. For this model Eq. (24) represents the solution of Eq. (10), and hence, the solution of Eq. (11) was obtained using Eq. (28) and Appendix ,

$$\Omega_{DE}^*(z) = C(z) + D(z)L(z) \int_{-1}^x \sum_{n=0}^2 \omega_n T_n(\tilde{x}) \frac{\tilde{A}(\tilde{x})F(\tilde{x})}{G(\tilde{x})} d\tilde{x}, \quad (29)$$

where the following relations were defined

$$C(z) = \Omega_{DE,0}(1+z)^3 \exp\left(\frac{3z_{max}}{2} \sum_{n=0}^2 \omega_n I_n(z)\right),$$

$$D(z) = \frac{z_{max}}{2} \Omega_{DM,0}(1+z)^{3(\omega_o - \omega_1 + \omega_2 + 1)},$$

$$F(\tilde{x}) = \exp\left[-3\left(\omega_1\left(1 + \frac{z_{max}}{2}[1+\tilde{x}]\right) + \omega_2\left(1 + \frac{z_{max}}{2}[1-\tilde{x}]\right)^2\right)\right],$$

$$G(\tilde{x}) = \left[1 + \frac{z_{max}}{2}(1+\tilde{x})\right]^{1-3(\omega_1 - \omega_2 - \omega_o)},$$

$$L(z) = \exp\left[3\left(\omega_2 z^2 + (\omega_1 - 2\omega_2)z + \omega_1 + \omega_2\right)\right].$$

Within this model, the function  $E^2$  was constructed from Eqs. (8)-(9), (24), (29) and (6). Furthermore, the relation

$$\omega'(z) = \omega_1 + 4z\omega_2, \quad (30)$$

is replaced into Eqs. (14)-(15) and (13) to reconstruct  $q(z)$  and  $j(z)$ , respectively. The basic analytical expressions for  $I_n(x)$  and  $\tilde{I}_n(\tilde{x})$  are found in Appendix .

## IV. CURRENT OBSERVATIONAL DATA AND COSMOLOGICAL CONSTRAINTS.

In this section, we describe how we use the cosmological data currently available to test and constrain the parameter space of our models proposed.

### A. Type Ia supernovae data set.

For the SNIa observations, we consider ‘‘The Supernova Cosmology Project’’ Union 2.1 composed of 580 SNIa data. The distance modulus  $\mu(z, \mathbf{X})$ , is defined as the difference between the apparent ( $m$ ) and absolute ( $M$ ) magnitudes, so that their observed and theoretical values are

$$\mu^{\text{obs}} = m^{\text{obs}} - M, \quad (31)$$

$$\mu^{\text{th}}(z, \mathbf{X}) \equiv 5 \log_{10} \left[ \frac{D_L(z, \mathbf{X})}{\text{Mpc}} \right] + \mu_0, \quad (32)$$

where  $\mu_0 = 25 - \log_{10} H_0$ , and the Hubble-free the luminosity distance  $D_L$  [1] in a flat cosmology is

$$D_L(z, \mathbf{X}) = (1+z) \int_0^z \frac{dz'}{H(z', \mathbf{X})}, \quad (33)$$

in where  $H(z, \mathbf{X})$  is the Hubble parameter, i.e., Eq. (6) and, in general,  $\mathbf{X}$  represents the model parameters

$$\mathbf{X} \equiv (H_0, \Omega_{b,0}, \Omega_{r,0}, \Omega_{DM,0}, \omega_o, \omega_1, \omega_2, \lambda_0, \lambda_1, \lambda_2). \quad (34)$$

The best fitting values of the parameters in a model are determined by the likelihood analysis of

$$\chi_{\text{SN}}^2(\mathbf{X}, m_0) \equiv \sum_{k=1}^{580} \frac{[\mu^{\text{obs}}(z_k) - \mu^{\text{th}}(z_k, \mathbf{X})]^2}{\sigma_k^2(z_k)}, \quad (35)$$

in where  $\sigma(z_k)$  is the corresponding  $1\sigma$  error of distance modulus for each supernovae. The parameter  $\mu_0$  is a nuisance parameter. According to [3],  $\chi^2$  is expanded as

$$\chi_{\text{SN}}^2(\mathbf{X}) = A_1 - 2\mu_0 B_1 + \mu_0^2 C_1, \quad (36)$$

where

$$\begin{aligned} A_1 &= \sum_{k=1}^{580} \frac{[\mu^{\text{obs}}(z_k) - \mu^{\text{th}}(z_k, \mathbf{X})]^2}{\sigma_k^2(z_k)}, \\ B_1 &= \sum_{k=1}^{580} \frac{[\mu^{\text{obs}}(z_k) - \mu^{\text{th}}(z_k, \mathbf{X})]}{\sigma_k^2(z_k)}, \\ C_1 &= \sum_{k=1}^{580} \frac{1}{\sigma_k^2(z_k)}. \end{aligned} \quad (37)$$

The Eq.(36) has a minimum for  $\mu_0 = B_1/C_1$  at

$$\tilde{\chi}_{\text{SN}}^2(\mathbf{X}) = A_1(\mathbf{X}) - \frac{B_1^2(\mathbf{X})}{C_1(\mathbf{X})}. \quad (38)$$

Since  $\chi_{\text{SN},\text{min}}^2 = \tilde{\chi}_{\text{SN},\text{min}}^2$ , instead minimizing  $\chi_{\text{SN}}^2$  we will minimize  $\tilde{\chi}_{\text{SN}}^2$ , which is independent of  $\mu_0$ .

## B. BAO data sets

Eisenstein et al.[5], first found a well-detected peak of the imprint of the recombination-epoch acoustic oscillations in the large-scale correlation function at  $100h^{-1}\text{Mpc}$  ( $h \equiv H_0/100\text{Kms}^{-1}\text{Mpc}^{-1}$ ) separation measured from a spectroscopic sample of 46,748 luminous red galaxies of the SDSS. Also, Percival et al.[7], investigated the clustering of galaxies within the spectroscopic SDSS-DR7 galaxy sample including, the luminous red galaxy, main samples, and also the 2-degree Field Galaxy Redshift Survey (2dFGRS) data (in total 893,319 galaxies) observed BAO in power spectrum of matter fluctuations after the epoch of recombination on large scales. This allowed to detect the BAO signal at  $z = 0.2$  and  $z = 0.35$ .

Eisenstein first and Percival after constructed an effective distance ratio  $D_v(z)$ , which encodes the visual distortion of a spherical object due to the non-Euclidianity of a FRW spacetime, defined as

$$\begin{aligned} D_v(z, \mathbf{X}) &\equiv \frac{1}{H_0} \left[ (1+z)^2 D_A^2(z) \frac{cz}{E(z)} \right]^{1/3}, \\ &= \frac{c}{H_0} \left[ \left( \int_0^z \frac{dz'}{E(z', \mathbf{X})} \right)^2 \frac{z}{E(z, \mathbf{X})} \right]^{1/3} \end{aligned} \quad (39)$$

$z$	$d_z$
0.20	$0.1905 \pm 0.0061$
0.35	$0.1097 \pm 0.0036$

TABLE I. Summary of SDSS-2dFGS BAO data set [7].

where  $D_A(z)$  is the proper (not comoving) angular diameter distance, which has the following definition

$$D_A(z, \mathbf{X}) \equiv \frac{c}{(1+z)} \int_0^z \frac{dz'}{H(z', \mathbf{X})}. \quad (40)$$

The comoving sound horizon size is defined by

$$r_s(a) \equiv c \int_0^a \frac{c_s(a') da'}{a'^2 H(a')}, \quad (41)$$

being  $c_s(a)$  the sound speed of the photon-baryon fluid

$$c_s^2(a) \equiv \frac{\delta P}{\delta \rho} = \frac{1}{3} \left[ \frac{1}{1 + (3\Omega_b/4\Omega_r)a} \right]. \quad (42)$$

Considering the Eqs. (41) and (42) for a  $z$  given

$$r_s(z) = \frac{c}{\sqrt{3}} \int_0^{1/(1+z)} \frac{da}{a^2 H(a) \sqrt{1 + (3\Omega_{b,0}/4\Omega_{\gamma,0})a}}, \quad (43)$$

where  $\Omega_{b,0}$  and  $\Omega_{\gamma,0}$  are the present-day baryon and photon density parameters, respectively. In this paper, we have fixed  $\Omega_{\gamma,0} = 2.469 \times 10^{-5} h^{-2}$ ,  $\Omega_{b,0} = 0.02246 h^{-2}$ , given by the WMAP7 data [13] and  $\Omega_{r,0} = \Omega_{\gamma,0}(1 + 0.2271 N_{\text{eff}})$  with  $N_{\text{eff}}$  the effective number of neutrino species (here the standard value,  $N_{\text{eff}} = 3.04$  was chosen [13]). The peak position of the BAO depends on the ratio of  $D_v(z)$  to the sound horizon size at the drag epoch (where baryons were released from photons)  $z_d$ , which was obtained by using a fitting formula [5]:

$$z_d = \frac{1291(\Omega_{M,0} h^2)^{0.251}}{1 + 0.659(\Omega_{M,0} h^2)^{0.828}} (1 + b_1(\Omega_{b,0} h^2)^{b_2}), \quad (44)$$

where  $\Omega_{M,0} = \Omega_{DM,0} + \Omega_{b,0}$  and

$$\begin{aligned} b_1 &= 0.313(\Omega_{M,0} h^2)^{-0.419} [1 + 0.607(\Omega_{M,0} h^2)^{0.674}], \\ b_2 &= 0.238(\Omega_{M,0} h^2)^{0.223}. \end{aligned}$$

The distance ratio  $d_z$  at  $z = 0.2$  and  $z = 0.35$  extracted from the SDSS and 2dFGRS [5–7], are listed in Table I,

$$d_{0.20}(\mathbf{X}) = \frac{r_s(z_d)}{D_V(0.2, \mathbf{X})}, \quad d_{0.35}(\mathbf{X}) = \frac{r_s(z_d)}{D_V(0.35, \mathbf{X})}, \quad (45)$$

where  $r_s(z_d, \mathbf{X})$  is the comoving sound horizon size at the baryon drag epoch. Using the data of Table I, then the inverse covariance matrix of BAO [7] is

$$C_{\text{SDSS}}^{-1} = \begin{pmatrix} +30124 - 17227 & \\ -17227 + 86977 & \end{pmatrix}. \quad (46)$$

$z_{eff}$	$A(z)$
0.44	$0.474 \pm 0.034$
0.60	$0.442 \pm 0.020$
0.73	$0.424 \pm 0.021$

TABLE II. Summary of the effective redshifts  $z_{eff}$  and the corresponding measurements for the acoustic parameter  $A(z)$  of the WiggleZ BAO data [9].

The errors of the SDSS-2dFGS BAO data are contained in  $C_{\text{SDSS}}^{-1}$ . The  $\chi^2$  of the SDSS-2dFGS BAO data set is

$$\chi_{\text{SDSS}}^2(\mathbf{X}) = (\Delta d_i) (C_{\text{SDSS}}^{-1})_{ij} (\Delta d_j)^t, \quad (47)$$

where  $\Delta d_i = d_i^{th}(\mathbf{X}) - d_i^{obs}$  is a column vector

$$d_i^{th}(\mathbf{X}) - d_i^{obs} = \begin{pmatrix} d_{0.20}(\mathbf{X}) - 0.1905 \\ d_{0.35}(\mathbf{X}) - 0.1097 \end{pmatrix}, \quad (48)$$

and “t” denotes its transpose.

On the other hand, in the low redshift region ( $z < 1$ ), Beutler et al. studied the large-scale correlation function of the 6dFGS and detected a BAO signal [8]. This detection allowed to constrain the distance-redshift relation  $D_v(z)$  at  $z_{eff} = 0.106$ ,  $D_v(z_{eff}) = 456 \pm 27$  Mpc and a measurement of the distance ratio,  $d_{z_{eff}} = r_s(z_d)/D_v(z_{eff}) = 0.336 \pm 0.015$ , where  $r_s(z_d)$  is the sound horizon at the drag epoch  $z_d$ .

The  $\chi^2$  function of the 6dFGS BAO data set is given by

$$\chi_{\text{6dFGS}}^2(\mathbf{X}) = \left( \frac{d_z - 0.336}{0.015} \right)^2. \quad (49)$$

Also, in [9], Blake et al. presented new measurements of the BAO at  $z = 0.44, 0.6$ , and  $0.73$  in the galaxy correlation function of the final data set of the WiggleZ. This sample included a total of  $N = 158,741$  galaxies in the range  $0.2 < z < 1.0$ . Here, the acoustic parameter  $A$ , was defined as [5]:

$$A(z) \equiv D_v(z) \sqrt{\Omega_{M,0}} \left( \frac{H_0}{cz} \right), \\ = \sqrt{\Omega_{M,0}} \left( \left( \int_0^z \frac{dz'}{E(z', \mathbf{X})} \right)^2 \frac{1}{z^2 E(z, \mathbf{X})} \right)^{1/3} \quad (50)$$

Using the BAO data showed into Table II, the inverse covariance matrix of WiggleZ BAO [9] is given by

$$C_{\text{WiggleZ}}^{-1} = \begin{pmatrix} +1040.3 - 807.5 + 336.8 \\ -807.5 + 3720.3 - 1551.9 \\ +336.8 - 1551.9 + 2914.9 \end{pmatrix}. \quad (51)$$

Then, define the  $\chi^2$  function of the WiggleZ BAO data

$$\chi_{\text{WiggleZ}}^2(\mathbf{X}) = (\Delta A_i) (C_{\text{WiggleZ}}^{-1})_{ij} (\Delta A_j)^t, \quad (52)$$

where  $\Delta A_i = A_i^{th}(\mathbf{X}) - A_i^{obs}$  is a column vector

$$A_i^{th}(\mathbf{X}) - A_i^{obs} = \begin{pmatrix} A(0.44, \mathbf{X}) - 0.474 \\ A(0.60, \mathbf{X}) - 0.442 \\ A(0.73, \mathbf{X}) - 0.424 \end{pmatrix}, \quad (53)$$

$l_A(z_*)$	$302.09 \pm 0.76$
$R(z_*)$	$1.725 \pm 0.018$
$z_*$	$1091.3 \pm 0.91$

TABLE III. The distance priors given by [13].

and “t” denotes its transpose.

Since Eqs. (47), (49) and (52), the total  $\chi^2$  for the BAO data sets is constructed

$$\chi_{\text{BAO}}^2 = \chi_{\text{SDSS}}^2 + \chi_{\text{6dFGS}}^2 + \chi_{\text{WiggleZ}}^2. \quad (54)$$

### C. CMB data set

The Union 2.1 SNIa and BAO data sets contain information about the universe at low redshifts, we now include WMAP 7 data [13] to probe the entire expansion history up to the last scattering surface. The shift parameter  $\mathbf{R}$  is provided by [11]

$$\mathbf{R}(z_*, \mathbf{X}) \equiv \frac{H_0}{c} \sqrt{\Omega_{M,0}} (1 + z_*) D_A(z_*, \mathbf{X}), \\ = \sqrt{\Omega_{M,0}} \int_0^{z_*} \frac{d\bar{y}}{E(\bar{y})}, \quad (55)$$

where the distance  $D_A$  and  $E(\bar{y})$  are given by Eqs. (40) and (6), respectively. Then, the redshift  $z_*$  (the decoupling epoch of photons) was obtained using the following fitting function [10]

$$z_* = 1048 \left[ 1 + 0.00124 (\Omega_{b,0} h^2)^{-0.738} \right] \left[ 1 + g_1 (\Omega_{M,0} h^2)^{g_2} \right], \quad (56)$$

where  $\Omega_{M,0} = \Omega_{DM,0} + \Omega_{b,0}$ , moreover,  $g_1$  and  $g_2$  are

$$g_1 = \frac{0.0783 (\Omega_{b,0} h^2)^{-0.238}}{1 + 39.5 (\Omega_{b,0} h^2)^{0.763}}, \quad g_2 = \frac{0.560}{1 + 21.1 (\Omega_{b,0} h^2)^{1.81}}. \quad (57)$$

An angular scale  $l_A$  for the sound horizon at decoupling epoch was defined as

$$l_A(\mathbf{X}) \equiv (1 + z_*) \frac{\pi D_A(z_*, \mathbf{X})}{r_s(z_*, \mathbf{X})}, \quad (58)$$

where  $r_s(z_*, \mathbf{X})$  is the comoving sound horizon at  $z_*$ , and is given by Eq. (43). The maximum likelihood values according WMAP 7 data [13] are given in Table III.

Then, following [13] the  $\chi^2$  for the CMB data is

$$\chi_{\text{CMB}}^2(\mathbf{X}) = (\Delta x_i) (C_{\text{CMB}}^{-1})_{ij} (\Delta x_j)^t, \quad (59)$$

where  $\Delta x_i = x_i^{th}(\mathbf{X}) - x_i^{obs}$  is a column vector

$$x_i^{th}(\mathbf{X}) - x_i^{obs} = \begin{pmatrix} l_A(z_*) - 302.09 \\ R(z_*) - 1.725 \\ z_* - 1091.3 \end{pmatrix}, \quad (60)$$

“t” denotes its transpose and  $(C_{\text{CMB}}^{-1})_{ij}$  is the inverse covariance matrix ([13]) given by

$$C_{\text{CMB}}^{-1} \equiv \begin{pmatrix} +2.3050 & +29.6980 & -1.3330 \\ +29.698 & +6825.27 & -113.18 \\ -1.3330 & -113.180 & +3.4140 \end{pmatrix}. \quad (61)$$

The errors for the CMB data are contained in  $C_{\text{CMB}}^{-1}$ .

#### D. Observational Hubble data (H)

In [14–16], the authors established that it is possible to compute the observational Hubble data, by using differential ages of galaxies through the measuring of  $dz/dt$ . Then, the Hubble parameter was expressed in terms of the differential ages as

$$\mathbf{H}(z) = -\frac{1}{1+z} \frac{dz}{dt}. \quad (62)$$

Simon et al.[16] found Hubble data over the redshift range  $[0, 1.8]$ . In [17], the authors found new data of the Hubble parameter at  $z \in [0.35, 1]$  from SPICES and VVDS galaxy surveys, respectively, which are listed in Table IV. In addition, in [18], the authors took the BAO scale as a standard ruler in the radial direction and found three more additional data:  $H(z = 0.24) = 79.69 \pm 2.32$ ,  $H(z = 0.34) = 83.80 \pm 2.96$  and  $H(z = 0.43) = 86.45 \pm 3.27$  (in units of  $Kms^{-1}Mpc^{-1}$ ). The  $\chi^2$  for the observational Hubble data is [72]

$$\chi_H^2(\mathbf{X}) \equiv \sum_{i=1}^{15} \frac{[H^{\text{th}}(\mathbf{X}, z_i) - H^{\text{obs}}(z_i)]^2}{\sigma^2(z_i)}, \quad (63)$$

where  $\mathbf{X}$  represents the parameters of the model,  $H^{\text{th}}$  is the theoretical value for the Hubble parameter,  $H^{\text{obs}}$  is the observed value, and  $\sigma(z_i)$  is the standard deviation measurement uncertainty. Here the summation is over the 15 observational Hubble data at  $z_i$ . This test has been already used to constrain several models in [73–75]. Therefore, to fit our models with observations, we use all the data sets described above.

The best fitted parameters are obtained by minimizing

$$\tilde{\chi}^2 = \tilde{\chi}_{\text{SN}}^2 + \chi_{\text{BAO}}^2 + \chi_{\text{CMB}}^2 + \chi_{\text{H}}^2. \quad (64)$$

From (64), we will construct the total probability density function **pdf** as

$$\mathbf{pdf}(\mathbf{X}) = A e^{-\tilde{\chi}^2/2}. \quad (65)$$

where  $A$  is a integration constant.

#### E. Constant Priors

In this work, we have assumed that baryonic matter ( $b$ ) and radiation ( $r$ ) are not coupled to  $DE$  or  $DM$  and

are separately conserved [71]. In this regard, we believe that the intensity of the interaction,  $I_Q$ , is not affected by the values of  $\Omega_{b,0}$  and  $\Omega_{r,0}$ , respectively. Due to it, in this paper, we have fixed:  $\Omega_{\gamma,0} = 2.469 \times 10^{-5}h^{-2}$  and  $\Omega_{b,0} = 0.02246h^{-2}$ , given by WMAP 7 data [13]. Then, based in these assumptions, construct **pdf** for each of our models. The priors on the parameters space are given in Table V, which were used in all the observational tests of our models. They have allowed us to compute the best fitting values of the free parameters.

## V. RESULTS

In this section, we present the results of the fitting on the models listed in Table VI, using the Union 2.1 SNIa data set, the BAO data set, the CMB data from WMAP 7, the H data set and the priors described in Table V. Likewise, for the uncoupled  $\Lambda$ CDM and CPL models, the corresponding free parameters to be estimated are:  $\mathbf{X} = (\Omega_{DM,0}, H_0)$  and  $\mathbf{X} = (\Omega_{DM,0}, H_0, \omega_o, \omega_1)$ . Meanwhile, for the coupled XCPL and DR models the free parameters are:  $\mathbf{X} = (\Omega_{DM,0}, H_0, \omega_o, \omega_1, \lambda_0, \lambda_1, \lambda_2)$ ,  $\mathbf{X} = (\Omega_{DM,0}, H_0, \omega_o, \omega_1, \omega_2, \lambda_0, \lambda_1, \lambda_2)$ , respectively. In each model, the function  $\tilde{\chi}_{\text{min}}^2$ , the one-dimension probability contours, the best fitting parameters, and their errors at  $1\sigma$  and  $2\sigma$  were computed, by using the Bayesian statistic method, as are shown in Figures 1, 2 and 3, respectively.

The values of the functions  $q$ ,  $j$ ,  $I_Q$ ,  $\omega$  and  $\Omega_{DM}$  evaluated in  $z = 0$  (today) are denoted as  $q_o$ ,  $j_o$ ,  $I_o$ ,  $\omega_o$  and  $\Omega_{DM,0}$ , respectively, and are presented in Table VII. Furthermore, the coupled models show that the  $\omega = -1$  crossing feature is more favored by the reconstructed  $\omega$  in the DR model with two crossings in the past ( $z = 21.11$  and  $z = 7895$ ) than that found in the XCPL model with only one crossing in a recent epoch ( $z = 0.07$ ) [76]. These crossing points obtained from the best reconstructed  $\omega$  are illustrated in Figure 4.

Let us now see Figure 4, within the coupled models have considered that  $I_+$  denotes an energy transfer from  $DE$  to  $DM$ , instead,  $I_-$  denotes an energy transfer from  $DM$  to  $DE$ . A change of sign on the best reconstructed  $I_Q$  is linked to the crossing of the noncoupling line  $I_Q(z) = 0$ . In this regard, within the coupled models have found a change from  $I_+$  in the past to  $I_-$  in the present and vice versa. According to this Figure and Table VII note that a non-negligible value of  $I_0$  at  $1\sigma$  error has been found in the coupled models, and whose order of magnitude is in agreement with the results obtained in [55–59, 64].

Due to the two minimums obtained in each coupled model (see Table VI), then two different possibilities to reconstruct  $I_Q$  have been found here. Therefore, for any  $z$  range, an interesting mixture of  $I_+$  and  $I_-$  may be described there.

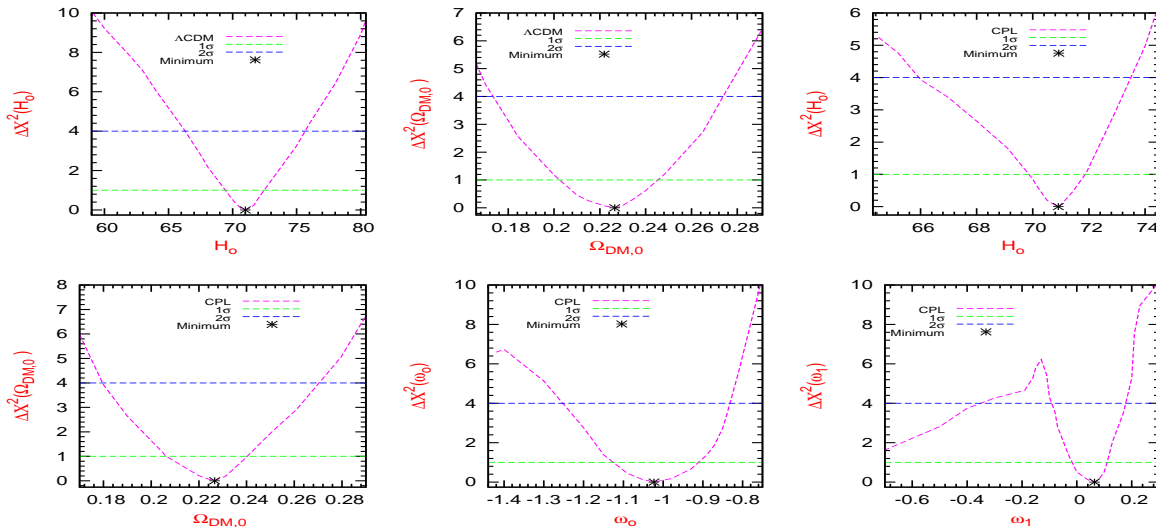
In what follows we compared both the results of the XCPL model with those of the CPL model, and also, the predictions of the DR model with the corresponding

$z$	$H(z)$	$1\sigma$
0.0	74.2	$\pm 3.6$
0.10	69	$\pm 12$
0.17	83	$\pm 8$
0.27	77	$\pm 14$
0.40	95	$\pm 17$
0.48	97	$\pm 60$
0.88	90	$\pm 40$
0.90	117	$\pm 23$
1.30	168	$\pm 17$
1.43	177	$\pm 18$
1.53	140	$\pm 14$
1.73	202	$\pm 40$

TABLE IV. Shows the observational  $H(z)$  data [17].

Parameters	Constant Priors
$\Omega_{DM,0}$	$[0, 0.7]$
$H_0(kms^{-1}Mpc^{-1})$	$[20, 140]$
$\lambda_0$	$[-1.5 \times 10^{+6}, +1.5 \times 10^{+6}]$
$\lambda_1$	$[-1.5 \times 10^{+6}, +1.5 \times 10^{+6}]$
$\lambda_2$	$[-1.5 \times 10^{+6}, +1.5 \times 10^{+6}]$
$\omega_o$	$[-2.0, -0.3]$
$\omega_1$	$[-1.0, +1.0]$
$\omega_2$	$[-10, +10]$

TABLE V. Shows the priors on the parameter space.

FIG. 1. (color online) Shows the one-dimension probability contours for each of the parameters of our noncoupled models. In each panel the black star denotes the best fitting value of the parameters. The  $1\sigma$  and  $2\sigma$  represent the errors.

of the  $\Lambda$ CDM model. Otherwise, according to the results presented in Figures 4 and 5. For  $z \geq 3.98$  the values of the amplitudes of  $\Omega_{DM}$  in the coupled models are slightly modified by the values of  $I_Q$  ( $I_+$  or  $I_-$ ) when they are compared with the uncoupled models. For  $I_+ > 0$ , the amplitudes of  $\Omega_{DM}$  are amplified, instead, for  $I_- < 0$ , these amplitudes are suppressed. These results coincide with those found in [53]. In addition, in any another  $z$  region, these effects are not possible. They are described in Table VIII (left and center above table), in where the  $z$  ranges and the coupled models are indicated. Likewise, we have also noted that, the shape of  $\Omega_{DE}$  and the values of its amplitudes are not significantly affected by the reconstructions of  $I_Q$  and  $\omega$  with respect to uncoupled models. Furthermore, we also confirm that the coincidence problem is alleviated in these coupled models, but they may not solve it. The below panels in Figure 5, as well as, the right above panel and below panels in Figures 6 and 7, the constraints at  $1\sigma$  and  $2\sigma$  on  $\Omega_{DM}$ ,  $\Omega_{DE}$ ,  $I_Q$ ,  $\omega$ ,  $q$  and  $j$  have been omitted to obtain a better visuali-

zation of these effects.

From Figure 6 (left above panel) our coupled models have predicted that a transition from a deceleration era at early times to an acceleration era at late times has been reached by the universe and the redshift for this change,  $z_T$ , is found to be  $z_T \sim 0.75$ .

Then, at  $z \rightarrow -1$  the DR model cannot determine, if the big-rip [77] may or may not occur in the universe, instead, for the XCPL model the universe will finish in a big-rip. These results coincide with those obtained in [38]. However, from Figure 6 (left above panel) and Table VIII (right above table) our results in the XCPL model have revealed that in determined  $z$  intervals the amplitude of  $q$  is slightly enhanced due to the increasing of the magnitudes of  $I_Q$  and  $\omega$  (see right above panel and below panels in Figure 6) with respect to that of the CPL model. Such a effect was realized when  $\Omega_{DM}$  becomes less concentrated at  $\log(z) \in [-2, +0.3]$  (see left panel in Figure 5). It was the epoch of the  $DE$  dominance, from which, the universe was led to an accelerated expansion.

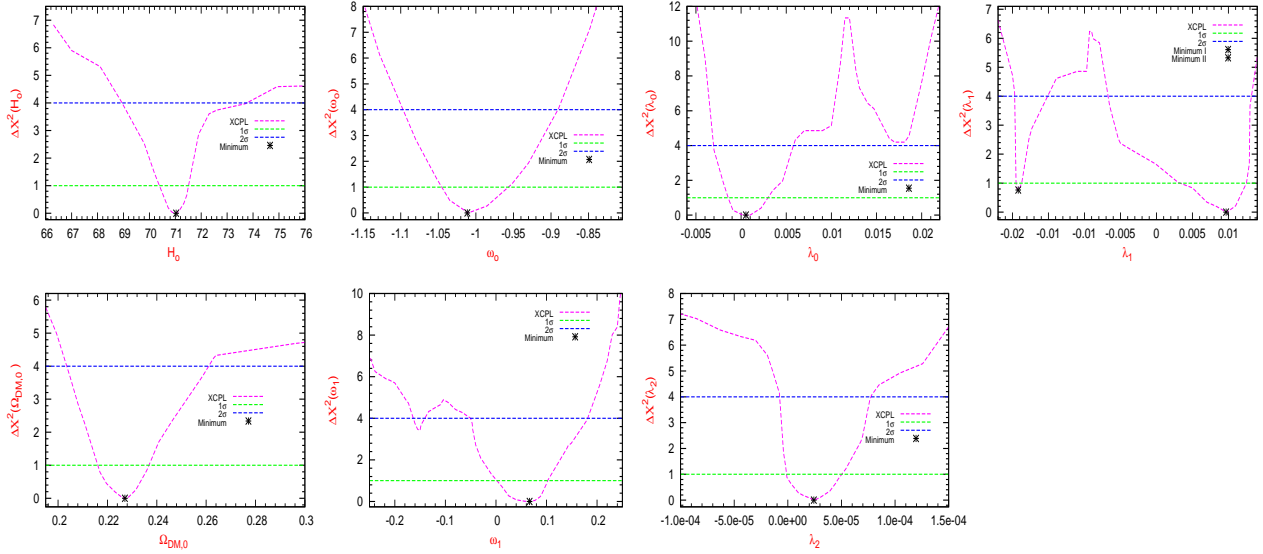


FIG. 2. (color online) Displays the one-dimension probability contours for the parameters of the XCPL model and their constraints at  $1\sigma$  and  $2\sigma$ , respectively. In each panel the black star denotes the best fitting parameter.

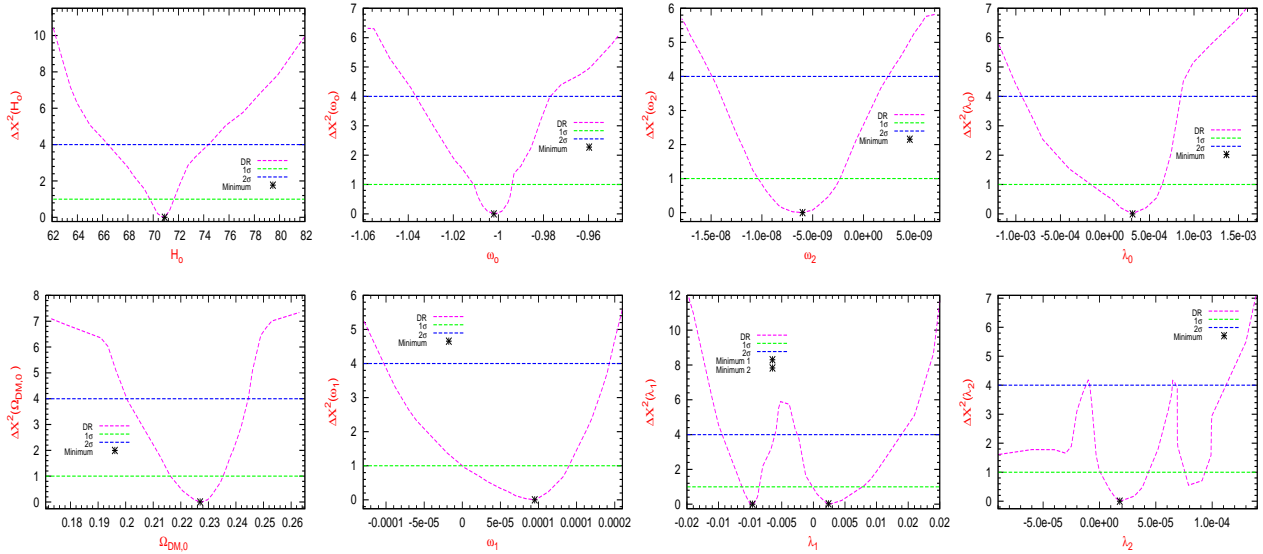


FIG. 3. (color online) Displays the one-dimension probability contours for the parameters of the DR model and their constraints at  $1\sigma$  and  $2\sigma$ , respectively. In each panel the black star denotes the best fitting parameter.

Regarding Figure 7 (left above panel), we have found qualitatively different asymptotic values in the near future ( $z \rightarrow -1$ ), but similar asymptotic values in the past ( $z \gg 1$ ) are exhibited by the best reconstructed  $j$ . Now let us analyze this Figure (right upper panel and lower panels) and Table VIII (below tables), from which, note that the magnitudes of  $I_Q$  and  $\omega$  have imprinted new physical effects on the amplitudes of the parameter  $j$ . Within the coupled models the amplitudes of  $j$  were progressively increased or reduced in determined  $z$  regions, with respect to those of the uncoupled models for increasing of the magnitudes of  $I_Q$  and  $\omega$ . Furthermore,

the expansion of the universe was modified by the consequent diminution of  $\Omega_{DM}$ . Therefore, we have shown that the magnitudes of  $I_Q$  and  $\omega$  are strongly related with the magnitudes of  $\Omega_{DM}$ ,  $q$  and  $j$ , respectively, as are seen in Figures 5, 6 and 7.

We now compare our results with those obtained by other researchers. In [65] several parametrizations for  $\omega$  were proposed, and also, a series for  $\omega$  in [66] (see Tables 1 and 2), was investigated, and then, compared it with an expansion of the scale factor up to the fifth order. The results of [65] and [66] are comparable with our results at  $1\sigma$  error (see Table VII). Furthermore, in [67] and [68]

TABLE VI. Shows the best fitting cosmological parameters for each model, and their constraints at  $1\sigma$  and  $2\sigma$ , obtained from an analysis of Union 2.1 SNIa+BAO+CMB+H data sets.

Parameters	$\Lambda$ CDM	CPL	XCPL(I)
$\lambda_0$	N/A	N/A	$+0.536 \times 10^{-3} + 2.356 \times 10^{-3} + 5.249 \times 10^{-3}$ $-2.036 \times 10^{-3} - 3.643 \times 10^{-3}$
$\lambda_1$	N/A	N/A	$+9.68 \times 10^{-3} + 2.720 \times 10^{-3} + 3.420 \times 10^{-3}$ $-6.470 \times 10^{-3} - 16.376 \times 10^{-3}$
$\lambda_2$	N/A	N/A	$+2.43 \times 10^{-5} + 2.641 \times 10^{-5} + 5.284 \times 10^{-5}$ $-2.644 \times 10^{-5} - 3.287 \times 10^{-5}$
$\omega_o$	-1.0	$-1.0231^{+0.1118+0.1916}_{-0.1033-0.2299}$	$-1.0040^{+0.0453+0.1140}_{-0.0435-0.0947}$
$\omega_1$	N/A	$+0.0642^{+0.0465+0.1129}_{-0.0842-0.1592}$	$+0.0665^{+0.0353+0.1148}_{-0.0638-0.1183}$
$\omega_2$	N/A	N/A	N/A
$\Omega_{DM,0}$	$+0.2265^{+0.0187+0.0475}_{-0.0241-0.0533}$	$+0.2266^{+0.0194+0.0440}_{-0.0205-0.0470}$	$+0.2271^{+0.0094+0.0314}_{-0.0132-0.0227}$
$H_0(kms^{-1}Mpc^{-1})$	$+70.9963^{+1.5049+4.6282}_{-1.6108-4.6937}$	$+70.9060^{+0.9572+2.5967}_{-1.0491-4.9753}$	$+71.0321^{+0.4785+2.7324}_{-0.6659-2.1272}$
$\chi^2_{min}$	567.5023	559.68457	557.87849

Parameters	XCPL(II)	DR(1)	DR(2)
$\lambda_0$	$+0.536 \times 10^{-3} + 2.356 \times 10^{-3} + 5.249 \times 10^{-3}$ $-2.036 \times 10^{-3} - 3.643 \times 10^{-3}$	$+3.1 \times 10^{-4} + 3.3243 \times 10^{-4} + 5.4365 \times 10^{-4}$ $-4.7626 \times 10^{-4} - 12.4271 \times 10^{-4}$	$+3.1 \times 10^{-4} + 3.3243 \times 10^{-4} + 5.4365 \times 10^{-4}$ $-4.7626 \times 10^{-4} - 12.4271 \times 10^{-4}$
$\lambda_1$	$-19.2 \times 10^{-3} + 0.5 \times 10^{-3} + 4.0 \times 10^{-3}$ $-0.4 \times 10^{-3} - 0.5 \times 10^{-3}$	$-9.62 \times 10^{-3} + 1.07 \times 10^{-3} + 3.5825 \times 10^{-3}$ $-1.5925 \times 10^{-3} - 4.78 \times 10^{-3}$	$+2.4 \times 10^{-3} + 5.314 \times 10^{-3} + 11.4036 \times 10^{-3}$ $-2.939 \times 10^{-3} - 4.9268 \times 10^{-3}$
$\lambda_2$	$+2.43 \times 10^{-5} + 2.641 \times 10^{-5} + 5.284 \times 10^{-5}$ $-2.644 \times 10^{-5} - 3.287 \times 10^{-5}$	$+1.8 \times 10^{-5} + 2.5496 \times 10^{-5} + 4.6683 \times 10^{-5}$ $-1.7264 \times 10^{-5} - 2.6510 \times 10^{-5}$	$+1.8 \times 10^{-5} + 2.5496 \times 10^{-5} + 4.6683 \times 10^{-5}$ $-1.7264 \times 10^{-5} - 2.6510 \times 10^{-5}$
$w_0$	$-1.0040^{+0.0453+0.1140}_{-0.0435-0.0947}$	$-1.0020^{+0.0082+0.0252}_{-0.0092-0.0346}$	$-1.0020^{+0.0082+0.0252}_{-0.0092-0.0346}$
$w_1$	$+0.0665^{+0.0353+0.1148}_{-0.0638-0.1183}$	$+9.5 \times 10^{-5} + 4.4857 \times 10^{-5} + 9.7620 \times 10^{-5}$ $-9.7914 \times 10^{-5} - 19.801 \times 10^{-5}$	$+9.5 \times 10^{-5} + 4.4857 \times 10^{-5} + 9.7620 \times 10^{-5}$ $-9.7914 \times 10^{-5} - 19.801 \times 10^{-5}$
$w_2$	N/A	$-6.0 \times 10^{-9} + 3.6395 \times 10^{-9} + 8.4502 \times 10^{-9}$ $-4.4308 \times 10^{-9} - 8.9306 \times 10^{-9}$	$-6.0 \times 10^{-9} + 3.6395 \times 10^{-9} + 8.4502 \times 10^{-9}$ $-4.4308 \times 10^{-9} - 8.9306 \times 10^{-9}$
$\Omega_{DM,0}$	$+0.2271^{+0.0094+0.0314}_{-0.0132-0.0227}$	$+0.2270^{+0.0085+0.0176}_{-0.0114-0.0269}$	$+0.2270^{+0.0085+0.0176}_{-0.0114-0.0269}$
$H_0(kms^{-1}Mpc^{-1})$	$+71.0321^{+0.4785+2.7324}_{-0.6659-2.1272}$	$+70.91^{+0.7514+3.4634}_{-1.1901-4.5339}$	$+70.91^{+0.7514+3.4634}_{-1.1901-4.5339}$
$\chi^2_{min}$	558.04200	556.85491	556.27088

TABLE VII. Shows the best fitting parameters today for each model,  $q_o$ ,  $j_o$ ,  $I_o$ ,  $\omega_o$  and  $\Omega_{DM,0}$ , and their errors at  $1\sigma$  and  $2\sigma$ , obtained from a combination of data.

Models	$q_o$	$j_o$	$I_o \times 10^4$	$\omega_o$	$\Omega_{DM,0}$
$\Lambda$ CDM	$-0.5932^{+0.0253+0.0633}_{-0.0331-0.0700}$	$-1.00017^{+1 \times 10^{-5} + 2 \times 10^{-5}}_{-0.0-2 \times 10^{-4}}$	0.0	-1.0	$-0.2265^{+0.0187+0.0475}_{-0.0241-0.0533}$
CPL	$-0.6181^{+0.1396+0.2604}_{-0.1454-0.3205}$	$-1.1478^{+0.2891+0.3985}_{-0.3092-0.8395}$	0.0	$-1.0231^{+0.1118+0.1916}_{-0.1033-0.2299}$	$+0.2266^{+0.0140+0.0440}_{-0.0094+0.0314}$
XCPL(I)	$-0.5967^{+0.0622+0.1622}_{-0.0668-0.1362}$	$-1.0892^{+0.1041+0.2047}_{-0.0813-0.2169}$	$-5.1141^{+23.299+51.964}_{-20.093-36.098}$	$-1.0040^{+0.0453+0.1140}_{-0.0435-0.0947}$	$+0.2271^{+0.0094+0.0314}_{-0.0132-0.0227}$
XCPL(II)	$-0.5967^{+0.0621+0.1622}_{-0.0669-0.1363}$	$-1.0793^{+0.1047+0.2045}_{-0.0835-0.2224}$	$+5.1141^{+23.299+51.964}_{-20.093-36.098}$	$-1.0040^{+0.0453+0.1140}_{-0.0435-0.0947}$	$+0.2271^{+0.0094+0.0314}_{-0.0132-0.0227}$
DR(1)	$-0.5945^{+0.0202+0.0474}_{-0.0250-0.0698}$	$-1.0036^{+0.0262+0.0783}_{-0.0306-0.1203}$	$+2.9200^{+3.0693+4.9697}_{-4.5900-12.162}$	$-1.0020^{+0.0082+0.0252}_{-0.0092-0.0346}$	$+0.2270^{+0.0085+0.0176}_{-0.0114-0.0269}$
DR(2)	$-0.5945^{+0.0202+0.0474}_{-0.0250-0.0698}$	$-1.0076^{+0.0246+0.0753}_{-0.0299-0.1198}$	$+2.9200^{+3.0693+4.9697}_{-4.5900-12.162}$	$-1.0020^{+0.0082+0.0252}_{-0.0092-0.0346}$	$+0.2270^{+0.0085+0.0176}_{-0.0114-0.0269}$

TABLE VIII. Shows the effects of the reconstructions of  $I_Q(z)$  and  $\omega$  on the parameters  $\Omega_{DM}$ ,  $q$  and  $j$  in determined  $z$  ranges.

Model	XCPL(I)/DR(2)	XCPL(II)/DR(1)	XCPL(I)/XCPL(II)
Effect Parameter	Enhancement on $\Omega_{DM}$	Suppression on $\Omega_{DM}$	Enhancement on $q$
$z$	$(+\infty \rightarrow +3.98)$	$(+\infty \rightarrow +3.98)$	$(+0.1 \rightarrow -0.7)$
$\omega$	--	--	$(-0.998 \rightarrow -1.159)$
$I_Q(I_-)$	--	$(-0.01 \rightarrow -0.1)$	$(-1.384 \rightarrow -6.24) \times 10^{-3}$
$I_Q(I_+)$	$(+0.01 \rightarrow +0.1)$	--	$(+1.504 \rightarrow 13.976) \times 10^{-3}$
$\Omega_{DM}$	$(+0.80 \rightarrow +0.85)$	$(+0.80 \rightarrow +0.70)$	$(0.178 \rightarrow 0)$
$q$	--	--	$(-0.7 \rightarrow -1.3)$

Model	DR(1)	XCPL(I)	XCPL(II)	DR(1)	DR(2)	XCPL(I)
Effect Parameter	Enhancement on $j$	Enhancement on $j$	Enhancement on $j$	Suppression on $j$	Suppression on $j$	Suppression on $j$
$z$	$(+8 \rightarrow 0.295)$	$(+1.723 \rightarrow 0.045)$	$(+8 \rightarrow 0.045)$	$(+0.295 \rightarrow -1.0)$	$(+8.0 \rightarrow -1.0)$	$(+8 \rightarrow +1.723)$
$\omega$	$(-1.001 \rightarrow -1.002)$	$(-0.980 \rightarrow -1.002)$	$(-0.982 \rightarrow -1.002)$	$(-1.0019 \rightarrow -1.0021)$	$(-1.0013 \rightarrow -1.0021)$	$(-0.9449 \rightarrow -0.9619)$
$I_Q \times 10^3$	$(-76.65 \rightarrow -2.524)$	$(+17.217 \rightarrow +0.968)$	$(-153.064 \rightarrow -0.320)$	$(-2.524 \rightarrow +9.92)$	$(+19.51 \rightarrow -2.09)$	$(+77.976 \rightarrow +17.217)$
$\Omega_{DM}$	$(+0.591 \rightarrow +0.346)$	$(+0.496 \rightarrow +0.258)$	$(+0.461 \rightarrow +0.241)$	$(+0.349 \rightarrow +0.051)$	$(+0.346 \rightarrow +0.003)$	$(+0.496 \rightarrow +0.388)$
$j$	$(-0.9953 \rightarrow -1.0)$	$(-0.9968 \rightarrow -1.0698)$	$(-0.9821 \rightarrow -1.0698)$	$(-1.0003 \rightarrow -1.0098)$	$(-1.0061 \rightarrow -1.0098)$	$(-0.9968 \rightarrow -1.0176)$

the values of  $q_o$  and  $j_o$  were estimated from a series, in where, new variables were defined to avoid the problem of divergence, for example, see both Table 2 in [67] and Tables I, II and III in [68], respectively. These results are

compatible at  $1\sigma$  error with those found in Table VII. Otherwise, constraints on  $q_o$  and  $j_o$  were established by the authors in [69] (see Table 2, series 2D and 3D) from a general expression of the BAO modes, and also, em-

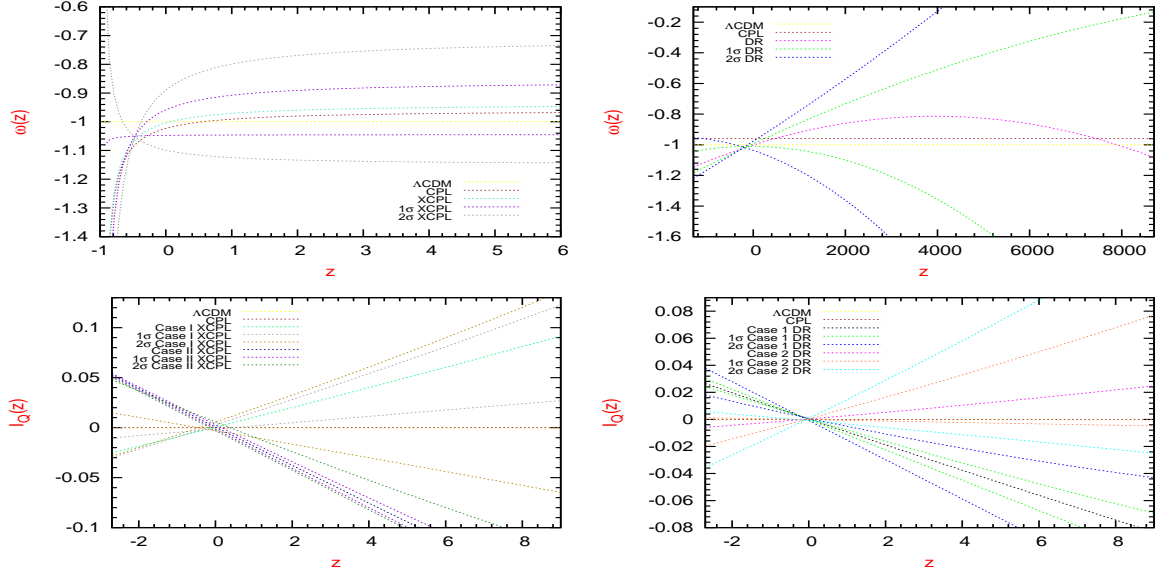


FIG. 4. (color online) The upper panels display the best reconstructed  $\omega(z)$  along  $z$ , their errors at  $1\sigma$  and  $2\sigma$  for the coupled models. These results are consistent with the  $\Lambda$ CDM model predictions. Similarly, The lower panels show the reconstructed evolution of  $I_Q$  and their errors at  $1\sigma$  and  $2\sigma$  in function of  $z$  for the coupled models and compared with the predictions of the uncoupled models.

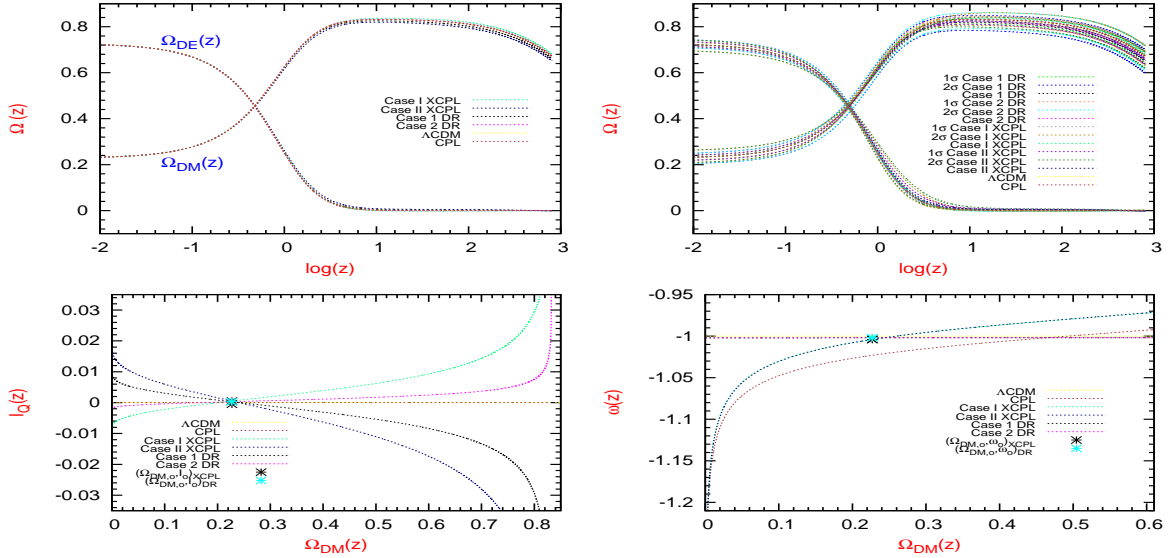


FIG. 5. (color online) The upper panels shows the best reconstructed energy densities at different  $z$  and their errors at  $1\sigma$  and  $2\sigma$  for the coupled models. Here, for  $z \geq 3.98$  and  $I_+$ , the values of the amplitudes of  $\Omega_{DM}$  are amplified, instead, at this same region and for  $I_- < 0$ , these amplitudes are suppressed with respect to the uncoupled models. The left below panel shows the evolution of  $I_Q$  as function of  $\Omega_{DM}$ . For  $\Omega_{DM} \geq 0.25$ , a disimination in the concentration of  $\Omega_{DM}$  implies that the amplitude of  $I_Q$  is increased and reduced in the coupled models, instead, for  $\Omega_{DM} < 0.25$ , it is always increased. Also, the right below panel shows the evolution of  $\omega$  as function of  $\Omega_{DM}$ . Here, a disimination of the values of  $\Omega_{DM}$  imply an increasing of the amplitude of  $\omega$ . Moreover, the “ $\sigma$ ” denotes the best fitting parameters in the present (see Table VII).

ploying a Taylor expansion and Padé approximations in [70] (see Table I, fourth column, fit 3). The results obtained in [69] and [70] at  $1\sigma$  are also consistent with those presented in Table VII.

## VI. CONCLUSIONS

Now we summarize our main results:

- An analysis combined of data was performed to break

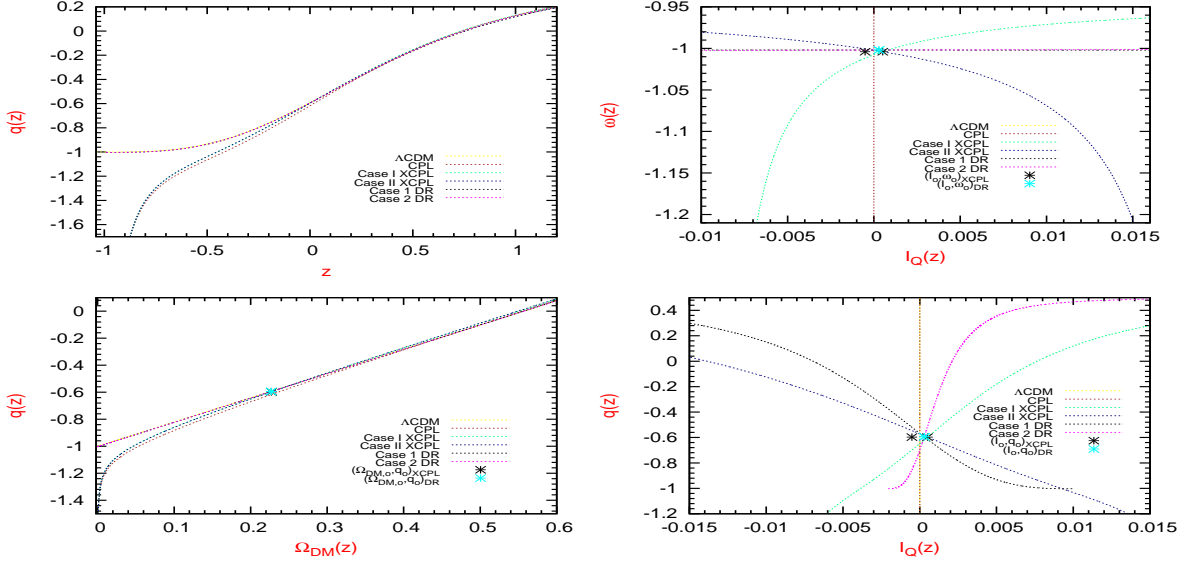


FIG. 6. (color online) The left above panel shows the evolution of  $q$  along  $z$ . The right panel displays the evolution of  $\omega$  as function of  $I_Q$ . Here, the magnitude of  $\omega$ ,  $|\omega|$  is enhanced from  $|-0.95|$  to  $|-1.2|$  when the values of  $I_Q$  moves from 0 to  $[0, 0.015]$ . The left and right below panels, depict the evolution of  $q$  as function of  $\Omega_{DM}$  and  $I_Q$ , respectively. Here, the magnitude of  $q$ ,  $|q|$ , is amplified from 0.1 to  $|-1.4|$  or from 0.4 to  $|-1.2|$ , when the values of  $\Omega_{DM}$  change from 0.6 to 0 or when the values of  $I_Q(z)$  moves from 0 to  $[0, 0.015]$ , respectively. Here, the “o” denotes the best fitting parameters in the present (see Table VII).

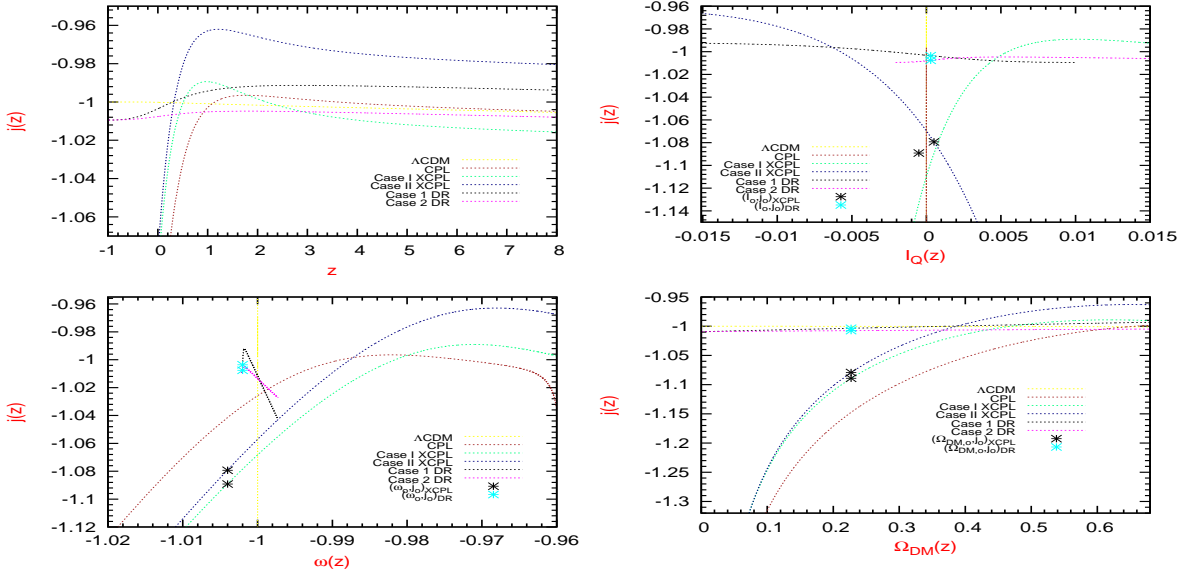


FIG. 7. (color online) The left above panel shows the evolution of  $j$  along  $z$ . The right panel displays the evolution of  $j$  as function of  $I_Q$ . Here, the magnitude  $|j|$ , is amplified from  $|-0.96|$  to  $|-1.14|$ , when the values of  $I_Q(z)$  moves from 0 to 0.005 and from 0 to  $-0.001$ , respectively. The left and right below panels, depict the evolution of  $j$  as function of  $\omega$  and  $\Omega_{DM}$ , respectively. Here, the magnitude  $|j|$ , is increased from  $|-0.96|$  to  $|-1.12|$  or from  $|-0.95|$  to  $|-1.3|$ , when the values of  $\omega$  moves from  $-0.96$  to  $-1.02$ , and also, when the values of  $\Omega_{DM}$  change from 0.7 to 0, respectively. The “o” denotes the best fitting values of the parameters in the present (see Table VII).

the degeneracy among the cosmological parameters of our models, allow us to obtain constraints more stringent on them. In particular, for the XCPL and DR models, the allowed region of its parameters was significantly reduced by the inclusion of the CMB data, compared with studies

of models without the CMB data [64, 78]. This implies that higher redshift may be able to discriminate between these models.

- In the DR model, a novel reconstruction for  $\omega$  was proposed whose best fitted value is closed to  $-1$ , and

has the property of avoiding divergences in a distant future  $z \rightarrow -1$ . This result is consistent with the value predicted by the  $\Lambda$ CDM model at  $1\sigma$  error. Likewise, within this scenario, a finite value for  $\omega$  has been obtained from the past to the future, mainly, the asymptotic values are:  $\omega(z) = \omega_2 z^2$  for  $z \gg 1$ ,  $\omega(z) \approx \omega_o$  for  $z \ll 1$  and  $\omega(z) \approx \omega_o$  for  $z \rightarrow -1$ . Therefore, a better physical description of the dynamical evolution of  $DE$  is performed by the DR model, which should be used to explore the properties of  $DE$ .

- Currently, a phase of accelerated expansion is the situation revealed by all our models about the universe. The big-rip problem is not forecasted by the DR model, and hence, this scenario should be considered to study the ultimate destiny of the universe. Likewise, from the coupled models found that the values of the amplitudes of the parameter  $q$  are not significantly affected neither by values of  $I_Q$  nor by the values of  $\omega$  (see left above panel in Figure 6).

- The values of the amplitudes of  $\Omega_{DE}$  (see upper panels in Figure 5) are not significantly modified by the reconstructions of  $I_Q$  and  $\omega$ , respectively, nevertheless, they are definitely positive. This requirement implies that  $\omega$  must be always negative in all the cosmic stages of the universe (see upper panels in Figure 4).

- The coupled models are strongly favored by the observational data having a preference for  $j_0 < -1$ , and hence, they represent a slight deviation from the value predicted

by the  $\Lambda$ CDM model (see Table VII).

- The behaviours qualitatively presented here show that the graph of  $j$  has more possibility in discriminating the different coupled  $DE$  models, and therefore,  $j$  could be used to distinguish them (see left upper panel in Figure 7).

- The physical effects generated by the magnitudes of  $I_Q$  and  $\omega$  on the cosmological parameters could be understood, so: An energy transfer from  $DE$  to  $DM$  or vice versa inserts energy into one of the fluids, and determines an increase of the energy density on one of them, which increases the Hubble parameter inducing a slight expansion of the universe, and to recover equilibrium of the system  $I_Q$  and  $\omega$  leads to an enhancement or suppression on the amplitudes and shapes of  $\Omega_{DM}$ ,  $q$  and  $j$  with respect to uncoupled models, in determined redshift ranges.

In a forthcoming paper we will extend our study by applying cosmological perturbation theory on the coupled models, using data of linear matter power spectrum, weak lensing potential, integrated Sachs-Wolfe, growth rate, and other. They will allow us to calculate of how the magnitudes of  $I_Q$  and  $\omega$  operate on the amplitudes of  $\Omega_{DM}$ ,  $q$  and  $j$ , respectively. From which, we may conclude if our DR model can emerge as an alternative to the  $\Lambda$ CDM model. This will be the purpose of our future work.

#### Appendix: Integrals $I_n(z)$ and $\tilde{I}_n(\tilde{x})$

$$I_0(z) = \frac{2}{z_{max}} \left[ \ln(1+z) \right], \quad (\text{A.1})$$

$$I_1(z) = \frac{2}{z_{max}} \left[ \frac{2z}{z_{max}} - \frac{(2+z_{max})}{z_{max}} \ln(1+z) \right], \quad (\text{A.2})$$

$$I_2(z) = \frac{2}{z_{max}} \left[ \frac{4z}{z_{max}} \left( \frac{z}{z_{max}} - \frac{2}{z_{max}} - 2 \right) + \left( 1 + \frac{6.828427}{z_{max}} \right) \left( 1 + \frac{1.171572}{z_{max}} \right) \ln(1+z) \right], \quad (\text{A.3})$$

$$\tilde{I}_0(\tilde{x}) = \frac{2}{z_{max}} \left[ \ln \left( 1 + 0.5 z_{max}(1 + \tilde{x}) \right) \right], \quad (\text{A.4})$$

$$\tilde{I}_1(\tilde{x}) = \frac{2}{z_{max}} \left[ \left( 1 + \tilde{x} \right) - \frac{(2+z_{max})}{z_{max}} \ln \left( 1 + 0.5 z_{max}(1 + \tilde{x}) \right) \right], \quad (\text{A.5})$$

$$\tilde{I}_2(\tilde{x}) = \frac{2}{z_{max}} \left[ \left( 1 + \tilde{x} \right) \left( \tilde{x} - \frac{4}{z_{max}} - 3 \right) + \left( 1 + \frac{6.828427}{z_{max}} \right) \left( 1 + \frac{1.171572}{z_{max}} \right) \ln \left( 1 + 0.5 z_{max}(1 + \tilde{x}) \right) \right]. \quad (\text{A.6})$$

#### ACKNOWLEDGMENTS

The author is grateful to Prof. F. Astorga for his academic support and fruitful discussions in the early

stages of this research, thank Prof. O. Sarbach and Prof. L. Ureña for useful discussions and comments, respectively. This work was in beginning supported by the IFM-UMSNH.

[1] A.G. Riess et al., *Astron. J.* **116** (1998) 1009; S. Perlmutter et al; *Astrophys. J.* **517** (1999) 565; J.L. Tonry et al., *Astrophys. J.*

**659** (2007) 98; T.M. Davis et al., *Astrophys. J.* **666** (2007) 716;

- M. Kowalski et al., *Astrophys. J.* **686** (2008) 749.
- [2] R. Amanullah et al., *Astrophys. J.* **716** (2010) 712.
- [3] S. Nesseris and L. Perivolaropoulos, *J. Cosmol. Astropart. Phys.* **0702** (2007) 025.
- [4] N. Suzuki et al., *Astrophys. J.* **85** (2012) 746.
- [5] D. J. Eisenstein, W. Hu, *Astrophys. J.* **496** (1998) 605.
- [6] K. Abazajian et al., *Astron. J.* **126** (2003) 2081; *Astron. J.* **128** (2004) 502; *Astron. J.* **129** (2005) 1755; *Astrophys. J. Suppl.* **182** (2009) 543; M. Tegmark et al., *Phys. Rev. D* **69** (2004) 103501; *Phys. Rev. D* **74** (2006) 123507; D. J. Eisenstein et al., *Astrophys. J.* **633** (2005) 560.
- [7] B. A. Reid et al., *Mon. Not. Roy. Astron. Soc.* **401** (2010) 2148; *Mon. Not. Roy. Astron. Soc.* **404** (2010) 60.
- [8] F. Beutler et al., *arxiv: 1106.3366v1* **06** (2011) 16.
- [9] C. Blake et al., *Mon. Not. Roy. Astron. Soc.* **418** (2011) 1707-1724.
- [10] W. Hu and N. Sugiyama, *Astrophys. J.* **471** (1996) 542.
- [11] J. R. Bond, G. Efstathiou and M. Tegmark, *Mon. Not. Roy. Astron. Soc.* **291** (1997) L33.
- [12] C.L. Bennett et al., *Astrophys. J. Suppl.* **148** (2003) 1; D.N. Spergel et al., *Astrophys. J. Suppl.* **148** (2003) 175; *Astrophys. J. Suppl.* **170** (2007) 377; G. Hinshaw et al., *Astrophys. J. Suppl.* **180** (2009) 225; E. Komatsu et al., *Astrophys. J. Suppl.* **180** (2009) 330.
- [13] E. Komatsu et al., *Astrophys. J. Suppl.* **192** (2011) 18.
- [14] R. Jimenez and A. Loeb, *Astrophys. J.* **573** (2002) 37.
- [15] R. Jimenez, L. Verde, T. Treu and D. Stern, *Astrophys. J.* **593** (2003) 622.
- [16] J. Simon, L. Verde and R. Jimenez, *Phys. Rev. D* **71** (2005) 123001.
- [17] A. G. Riess et al., *Astrophys. J.* **699** (2009) 539; D. Stern, R. Jimenez, L. Verde, M. Kamionkowski, S. A. Stanford, *Astrophys. J. Suppl.* **188** (2010) 280; *J. Cosmol. Astropart. Phys.* **02** (2010) 8.
- [18] E. Gaztanaga, A. Cabre and L. Hui, *Mon. Not. Roy. Astron. Soc.* **399** (2009) 1663.
- [19] P. J. E. Peebles and B. Ratra, *Astrophys. J.* **325** (1988) L17.
- [20] P. J. E. Peebles and B. Ratra, *Rev. Mod. Phys.* **75** (2003) 559.
- [21] V. Sahni, *Lect. Notes Phys.* **653** (2004) 141.
- [22] E. J. Copeland, M. Sami and S. Tsujikawa, *Int. J. Mod. Phys. D* **15** (2006) 1753.
- [23] S. Weinberg, *Rev. Mod. Phys.* **61** (1989) 1.
- [24] V. Sahni and A. A. Starobinsky, *Int. J. Mod. Phys. D* **9** (2000) 373.
- [25] U. Seljak et al., *Phys. Rev. D* **71** (2005) 103515.
- [26] E. Rozo et al., *Astrophys. J.* **708** (2010) 645.
- [27] R. R. Caldwell, *Phys. Lett. B* **545** (2002) 23; S. Nojiri and S. D. Odintsov, *Phys. Lett. B* **562** (2003) 147; R. Gannouji, D. Polarski, A. Ranquest and A. A. Starobinsky, *J. Cosmol. Astropart. Phys.* **09** (2006) 016; X. Cheng, Y. Gong and E. N. Saridakis, *J. Cosmol. Astropart. Phys.* **04** (2009) 001.
- [28] E. Elizalde, S. Nojiri, and S. D. Odintsov *Phys. Rev. D* **70** (2004) 043539; Z. K. Guo, Y. S. Piao, X. M. Zang and Y. Z. Zhang, *Phys. Lett. B* **608** (2005) 177.
- [29] B. Ratra, and P. J. E. Peebles, *Phys. Rev. D* **37** (1988) 3406; K. Coble, S. Dodelson, and J. A. Frieman, *Phys. Rev. D* **55** (1997) 1851; R. R. Caldwell, R. Dave, and P. J. Steinhardt, *Phys. Rev. Lett.* **80** (1998) 1582.
- [30] C. Armendariz-Picon, V. Mukhanov, P. J. Steinhardt, *Phys. Rev. Lett.* **85** (2000) 4438, *Phys. Rev. D* **63** (2001) 103510; T. Chiba, T. Okabe, M. Yamaguchi, *Phys. Rev. D* **62** (2000) 023511.
- [31] A. Y. Kamenshchik, U. Moschella and V. Pasquier, *Phys. Lett. B* **511** (2001) 265; M. C. Bento, O. Bertolami and A. A. Sen, *Phys. Rev. D* **66** (2002) 043507; M. K. Mak and T. Harko, *Phys. Rev. D* **71** (2005) 104022;
- [32] M. R. Garousi, M. Sami, S. Tsujikawa, *Phys. Lett. B* **606** (2005) 1; M. R. Garousi, M. Sami, and S. Tsujikawa, *Phys. Rev. D* **71** (2005) 083005.
- [33] A. R. Cooray and D. Huterer, *Astrophys. J.* **513** (1999) L95.
- [34] M. Chevallier, D. Polarski, *Int. J. Mod. Phys. D* **10** (2001) 213; E. V. Linder, *Phys. Rev. Lett.* **90** (2003) 091301
- [35] J. Barboza, E. M. and J. Alcaniz, *Phys. Lett. B* **666** (2008) 415.
- [36] E. M. Barboza Jr. et al; *Phys. Rev. D* **80** (2009) 043521.
- [37] Q. J. Zhang and Y. L. Wu, *J. Cosmol. Astropart. Phys.* **08** (2010) 038.
- [38] H. Li and X. Zhang, *Phys. Lett. B* **703** (2011) 119; J. Z. Ma and X. Zhang, *Phys. Lett. B* **699** (2011) 233.
- [39] T. Holsclaw et al, *Phys. Rev. Lett.* **105** (2010) 241302; T. Holsclaw et al, *Phys. Rev. D.* **84** (2011) 083501.
- [40] R. A. Daly and S. Djorgovski, *Astrophys. J.* **597** (2003) 009.
- [41] D. Huterer and A. Cooray, *Phys. Rev. D.* **71** (2005) 023506.
- [42] A. Shafieloo, U. Alam, V. Sahni and A. A. Starobinsky, *Mon. Not. R. Astron. Soc.* **366** (2006) 1081.
- [43] A. Hojjati, L. Pogosian and G. B. Zhao, *J. Cosmol. Astropart. Phys.* **04** (2010) 007.
- [44] O. Sarbach and M. Tiglio, *Liv. Rev. Rel.* **15** (2012) [gr-qc/1203.6443v1].
- [45] E. F. Martinez and L. Verde, *J. Cosmol. Astropart. Phys.* **08** (2008) 023.
- [46] M. S. Turner, *Phys. Rev. D* **28** (1983) 1243.
- [47] K. A. Malik, D. Wands, and C. Ungarelli, *Phys. Rev. D* **67** (2003) 063516.
- [48] R. Cen, *Astrophys. J.* **546** (2001) L77; M. Oguri, K. Takahashi, H. Ohno and K. Kotake, *Astrophys. J.* **597** (2003) 645.
- [49] Z. K. Guo, N. Ohta, and S. Tsujikawa, *Phys. Rev. D* **76** (2007) 023508.
- [50] C. G. Bohmer, G. Caldera-Cabral, R. Lazkoz, and R. Maartens, *Phys. Rev. D* **78** (2008) 023505.
- [51] J. Valiviita, E. Majerotto and R. Maartens, *J. Cosmol. Astropart. Phys.* **07** (2008) 020.
- [52] S. Campo, R. Herrera and D. Pavon, *J. Cosmol. Astropart. Phys.* **01** (2009) 020.
- [53] G. Caldera-Cabral, R. Maartens and B. M. Schaefer, *J. Cosmol. Astropart. Phys.* **07** (2009) 027.
- [54] L. P. Chimento, *Phys. Rev., D* **81** (2010) 043525.
- [55] E. Abdalla, L. R. Abramo and J. C. C. de Souza, *Phys. Rev. D* **82** (2010) 023508.
- [56] R. G. Cai and Q. Su, *Phys. Rev. D* **81** (2010) 103514.
- [57] J. H. He, B. Wang, and E. Abdalla, *Phys. Rev. D* **83** (2011) 063515.
- [58] S. Cao, N. Liang and Z. H. Zhu, *astro-ph.CO/1105.6274*.
- [59] Y. H. Li and X. Zhang, *Eur. Phys. J. C* **71** (2011) 1700.
- [60] W. Zimdahl, *Int. J. Mod. Phys. D* **14** (2005) 2319.
- [61] S. Das, P. S. Corasaniti, and J. Khoury, *Phys. Rev. D* **73** (2006) 083509.
- [62] G. Huey and B. D. Wandelt, *Phys. Rev. D* **74** (2006) 023519.
- [63] B. Wang, J. Zang, C. Y. Lin, E. Abdalla, and S. Micheletti, *Nucl. Phys. B* **778** (2007) 69.
- [64] F. Cueva Solano and U. Nucamendi, *J. Cosmol. Astropart. Phys.* **04** (2012) 011; F. Cueva Solano and U. Nucamendi, *arXiv: 1207.0250* **07** (2012) 02.
- [65] F. Y. Wang, Z. G. Dai, and Shi Qi, *Astronomy & Astrophysics.* **507** (2009) 53-59.
- [66] M. Demianski, E. Piedipalumbo, C. Rubano, P. Scudellaro, *Mon. Not. R. Astron. Soc.* **426** (2012) 1396-1415.
- [67] V. Vitagliano, J. Q. Xia, S. Liberati and M. Viel, *J. Cosmol. Astropart. Phys.* **03** (2010) 005.
- [68] A. Aviles, C. Gruber, O. Luongo, H. Quevedo, *Phys. Rev. D.* **86** (2012) 123516.
- [69] R. Lazkoz, J. Alcaniz, C. Escamilla-Rivera, V. Salzano, I. Sendra, *J. Cosmol. Astropart. Phys.* **12** (2013) 005.
- [70] C. Gruber and O. Luongo, *Phys. Rev. D.* **89** (2014) 103506.
- [71] Kazuya Koyama, Roy Maartens, and Yong-Seon Song, *J. Cosmol. Astropart. Phys.* **10** (2009) 017; P. Brax, C. van de Bruck, D. F. Mota, N. J. Nunes, and H. A. Winther, *Phys. Rev. D* **82** (2010) 083503.
- [72] R. Lazkoz and E. Majerotto, *J. Cosmol. Astropart. Phys.* **07** (2007) 015; J. Lu, L. Xu, M. Liu and Y. Gui, *Eur. Phys. J. C* **58** (2008) 311; L. Samushia and B. Ratra, *Astrophys. J.* **650** (2006) L5.
- [73] J. B. Lu, Y. X. Gui and L. X. Xu, *Eur. Phys. J. C* **63** (2009) 349.
- [74] L. X. Xu and J. B. Lu, *J. Cosmol. Astropart. Phys.* **03** (2010) 025.
- [75] L. Feng and Y. P. Yang, *Astron. Astrophys.* **11** (2011) 751.
- [76] S. Nesseris and L. Perivolaropoulos, *JCAP* **01** (2007) 018.
- [77] R. R. Caldwell, M. Kamionkowski and N. N. Weinberg, *Phys. Rev. Lett.* **91** 071301 (2003); L. P. Chimento and R. Lazkoz, *Mod. Phys. Lett. A* **19** 2479 (2004).
- [78] Xiao-Dong Xu, Jian-Hua He, Bin Wang, *Phys. Lett. B* **701** (2011) 513-519.